

UNIVERSITY OF TARTU
Faculty of Science and Technology
Institute of Physics

Moorits Mihkel Muru

**DETECTION OF WHIM STRUCTURE CANDIDATES IN THE
SDSS SPECTROSCOPIC SURVEY**

Master's thesis (30 ECTS)

Supervisors:
Jukka Henry Petteri Nevalainen, PhD
Elmo Tempel, PhD

Tartu 2018

Detection of WHIM structure candidates in the SDSS spectroscopic survey

A significant fraction of the local baryons as predicted by the Λ CDM cosmological model is not detected in surveys. One proposed solution to the missing baryons problem is that the matter is in form of diffuse Warm-Hot Intergalactic Medium (WHIM). Using correlation between luminosity and WHIM density (Nevalainen et al., 2015) we study a set of 64 lines of sight in Sloan Digital Sky Survey to trace WHIM structures. The sample was chosen representative enough to be able to make estimates on the whole sky. We searched for structures with high enough OVII column densities to be detectable with X-ray spectroscopy. For $N(OVII) > 10^{16} \text{cm}^{-2}$ our study found 3 structures and for $N(OVII) > 10^{15} \text{cm}^{-2}$ 44 structures, which agree with simulations. Estimates for the whole sky are 65 structures and 1135 structures respectively. This work is a preparation for compiling a WHIM structure finding map for future X-ray instruments like ARCUS and ATHENA.

Keywords: large-scale structure – filaments – WHIM – intergalactic medium – observations – simulation – X-ray spectroscopy

CERCS: P520 – Astronomy, space research, cosmic chemistry

WHIM struktuuride detekteerimine SDSS spektroskoopilistest vaatlusandmestest

Märkimisväärsed osa Λ CDM kosmoloogia poolt ennustatavatest kohaliku Universumi barüonidest pole siamaani suudetud vaatlustega tuvastada. Üks võimalikke lahendusi on, et need barüonid on hajusa sooja-kuuma gaasi (WHIM) kujul galaktikatevahelises ruumis. Kasutades heledustiheduse ja WHIM tiheduse vahelist korrelatsiooni (Nevalainen et al., 2015) uurime 64 vaatesihtiga kasutades Sloani taevaülevaate andmeid. Valimi määramisel peeti silmas, et see oleks piisavalt esinduslik, et teha selle põhjal eeldusi kogu taevaalaotuse jaoks. Me otsisime struktuure, mille OVII sambatihedus oleks piisavalt suur, et seda on võimalik röntgeni piirkonnas tuvastada. Sambatiheduse $N(OVII) > 10^{16} \text{cm}^{-2}$ jaoks tuvastasime 3 objekti ja $N(OVII) > 10^{15} \text{cm}^{-2}$ jaoks 44 objekti, mis lähevad hästi kokku simulatsioonide tulemustega. Hinnang kogu taevaalaotuse jaoks vastavalt sambatiheduse alumisele piirile 65 ja 1135 objekti. Selle uuringu eesmärk on aidata ettevalmistada kataloogi, mille abil tulevastele röntgenteleskoopidele (ARCUS ja ATHENA) vaatlusi komplekteerida.

Märksõnad: suureskaalaline struktuur – filamendid – WHIM – galaktikatevaheline gaas – vaatlused – simulatsioon – röntgen spektroskoopia

CERCS: P520 – Astronoomia, kosmoseuuritud, kosmosekeemia

Contents

Introduction	5
1 Theoretical overview	6
1.1 Missing baryons problem	6
1.2 Filaments	7
1.3 WHIM as a solution	8
1.3.1 Simulations	9
1.3.2 WHIM correlation with luminosity	11
2 Observational methods	12
2.1 Filament detection	12
2.2 Identifying and characterizing the luminosity density structures	14
2.2.1 Lines of sight	14
2.2.2 Crossing points	14
2.2.3 Structure identification from luminosity profiles	14
2.2.4 WHIM column density	15
2.2.5 Oxygen abundance in WHIM structures	16
3 Results	19
3.1 Structures	19
3.1.1 Crossing points	19
3.1.2 Luminosity profiles	20
3.2 WHIM column density distribution and structure count	22
3.3 Estimates for the whole sky	23
4 Simulation results and follow-up observations	25
4.1 Comparison to simulations	25
4.2 X-ray observations	26
Conclusion	28

Bibliography	30
Lihtlitsents	33

Introduction

The advance in observational instruments has led cosmology to have widely accepted precise predictions about the universe. The concordance cosmology, Λ CDM (Λ cold dark matter) model is a parametrization of the Big Bang cosmological model with cosmological constant Λ . It is used as the standard model of cosmology because it is the simplest theory that can explain Cosmic Microwave Background (CMB), distribution of matter in large-scale structures, the abundance of hydrogen, helium, and lithium, and the accelerating expansion of the universe observed as a redshift of distant objects.

The existence of the CMB is a very big argument in favour of Big Bang model in contrast to Steady State universe. This background blackbody radiation is evidence that universe was once very hot, dense, and opaque. As the universe expanded, it cooled. Today the CMB has temperature of 2.725 K (Komatsu et al., 2011). Analyzing the CMB very precise values for baryon density are obtained. Judging from observational data, a significant fraction of the baryons are missing (Shull et al., 2012; Cen, 2012). This leads to two options. Either the model is wrong or the baryons are in such form, that they are hard to detect with current instruments.

Knowing the environment is crucial for making correct predictions about the evolution of the universe and its components. Galactic properties, formation rate, and evolution are heavily affected by surrounding medium. Having unknown particles in the space impedes us from obtaining the true understanding of underlying processes. Therefore solving this bears utmost importance for many areas of cosmology, including cosmological model, large-scale structure, and galaxy evolution.

Chapter 1

Theoretical overview

1.1 Missing baryons problem

Analysis of Wilkinson Microwave Anisotropy Probe (WMAP) data for Cosmic Microwave Background (CMB) have found baryon matter-energy fraction to be $\Omega_b = 0.0455 \pm 0.0028$. Meaning that 4.6% of universe's energy is in baryons. Using the critical matter-energy density of the universe ($\rho_{\text{cr}} = 9.205 \times 10^{-30} \text{g cm}^{-3} h^2$, where $h = 70 \text{km s}^{-1} \text{Mpc}^{-1}$) the baryon mean comoving density can be calculated to be $\bar{\rho}_b = \Omega_b \rho_{\text{cr}} = 4.24 \times 10^{-31} \text{g cm}^{-3}$, and hydrogen number density assuming helium mass fraction 0.2477 $n_H = 1.90 \times 10^{-7} \text{cm}^{-3}$. (Komatsu et al., 2011)

The baryon composition in local universe is hard to determine due to the formation of galaxies and large-scale structure, and the feedback from star formation. Galaxy surveys have shown that about 7% of baryons are in galaxies, groups, and clusters. Approximately half of the remaining 80% of cosmic baryons are found to be in the intergalactic medium (IGM) in the form of gas (see figure 1.1). Far-ultraviolet spectroscopic surveys have detected lots of Ly α and OVI absorbers, but X-ray absorption by OVII has yet to confirm potential large reservoir of high temperature ($\log(T) > 6$) baryons, that are seen in simulations. (Shull et al., 2012) As the Λ CDM model agrees very well with most of the observations, it is more probable that there are missing baryons that are hard to detect with current instruments, rather than a flawed cosmological model. Even more so, because simulations predict hot baryons that have hard to detect footprints.

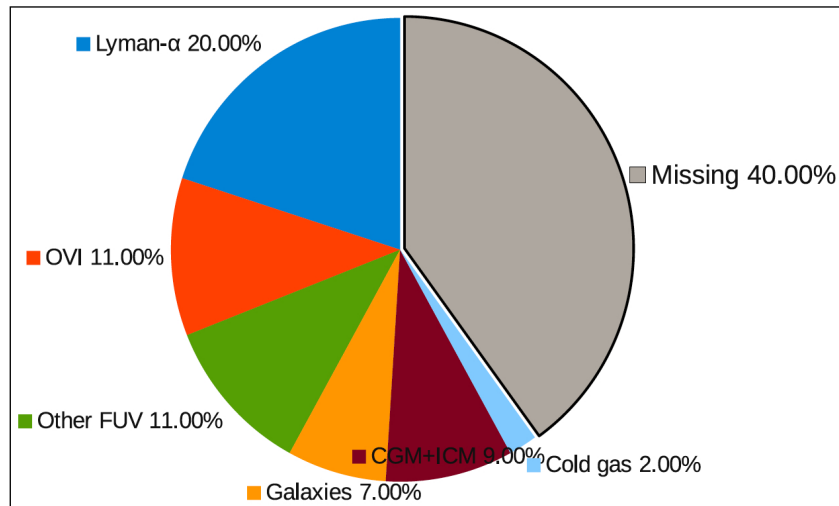


Figure 1.1: Baryon distribution in local universe. Lyman- α , OVI and other FUV are structures observable in ultraviolet band. Missing part is high-temperature X-ray gas. Galaxies, circumgalactic medium (CGM) and intercluster medium (ICM) represent collapsed baryon structures. Adapted from Shull et al. (2012).

1.2 Filaments

Large surveys of galaxies have shown the universe to have weblike structure (Jöeveer et al., 1978). The cosmic web consists of four basic structures of matter: elongated tube-like filaments, two-dimensional sheets, galaxy cluster in the connections of filaments and large almost empty voids between other structures. As the galaxy environment affects its properties, the underlying cosmic web has been the subject of numerous studies. The analysis is made more difficult by having no objective and quantitative way to identify these structures.

One way to describe the web is using velocity shear tensor, where velocity eigenvalues can be obtained. Each grid point will be identified certain structure element depending on how many eigenvalues are over set threshold. A higher value of velocity eigenvalue describes faster collapse of matter. That means three values over the threshold is a cluster, because it is collapsing in all three dimensions, two values over the threshold is filament, where collapsing is perpendicular to the elongation of filament, one value over the threshold is sheet, where collapsing is collinear to the normal of the sheet, and voids have no collapsing axis. The can be built along the vectors of the slowest collapse as seen in figure 1.2. (Libeskind et al., 2012, 2018)

Second identification relies on spatial galaxy distribution and statistical methods (Tempel et al., 2016). An object point process with interactions, named the Bisous model, fits filamentary network to a series of cylinders and improves the configuration with the Metropolis-Hasting

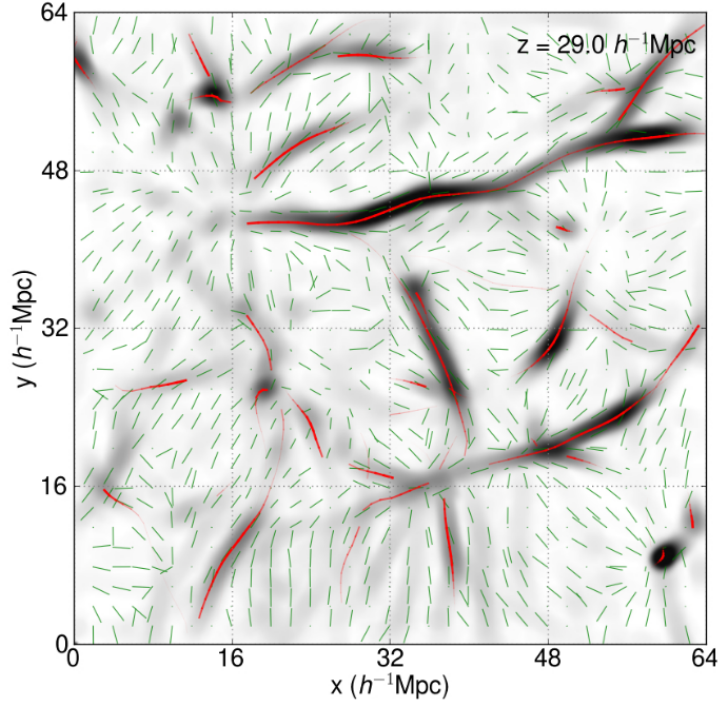


Figure 1.2: Constructing of cosmic web on velocity shear tensor. Projection of the vector of the slowest collapse (green) overlaid with filaments detected with Bisous model. (Tempel et al., 2014)

algorithm with annealing and tempering.

As filaments have higher mass density than the surrounding space, they are host to a lot of intergalactic gas. With the evolution of the universe, more and more matter falls into filaments, sheets, and clusters. Most of the baryons in local universe are expected to reside in filaments.

1.3 WHIM as a solution

A possible solution for the missing baryon problem is high-temperature diffuse gas. These are baryons that are not in collapsed objects such as galaxies, have high enough temperature to not be detectable in the far-ultraviolet band, and so diffuse that current X-ray measurements don't have good enough resolution to conduct a larger survey. Baryon gas with temperature $5 < \log(T)[K] < 7$ and mass overdensity $1 < \frac{\rho_b}{\langle \rho_b \rangle} < 100$ is named Warm-Hot Intergalactic Medium (WHIM) (Nevalainen et al., 2015) (see figure 1.3). Intergalactic medium in the filamentary network is heated up by shock-waves from cumulated gravitational potential. Baryons outside of filaments have less chance of being heated to sufficient temperatures. As gas enriched filaments are favourable for galaxy formation, therefore WHIM and galaxies inhabit the same underlying filaments and have a spatial correlation.

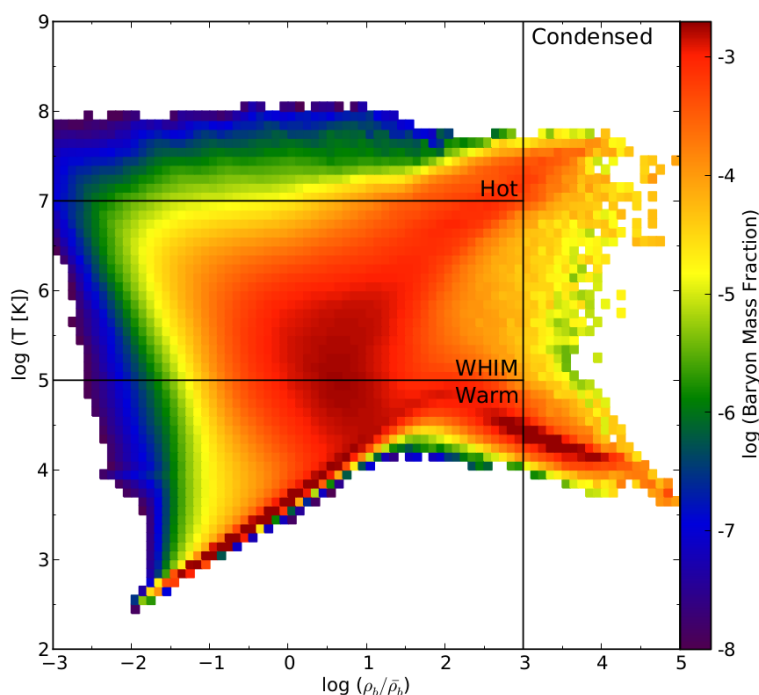


Figure 1.3: Intergalactic medium color-coded by baryon mass fraction. WHIM is defined to as temperature $5 < \log(T)[K] < 7$ and mass overdensity $1 < \frac{\rho_b}{\langle \rho_b \rangle} < 100$, having the highest baryon mass fraction. (Shull et al., 2012)

Higher temperature WHIM is hard to detect in spectroscopic surveys because low density of the gas renders the signal to the lower end of resolution for instruments available at the moment (e.g. XMM-Newton). Detecting WHIM also requires bright background source, such as blazars and Gamma Ray Bursts afterglows.

1.3.1 Simulations

As WHIM is hard to detect, much is learned from simulations. Some of the bigger and well-analyzed simulations are Cen (2012) and Shull et al. (2012). Both are a large-scale cosmological hydrodynamic simulation with adaptive mesh using both dark matter and baryon particles. These simulations confirm WHIM's spatial correlation with galaxy distribution and therefore filaments (see figure 1.4). Simulations also predict large fraction of intergalactic medium to be in hot state suitable for WHIM (see figure 1.5 and 1.6), and confirm that about 70% of baryons in filaments are WHIM (Nevalainen et al., 2015).

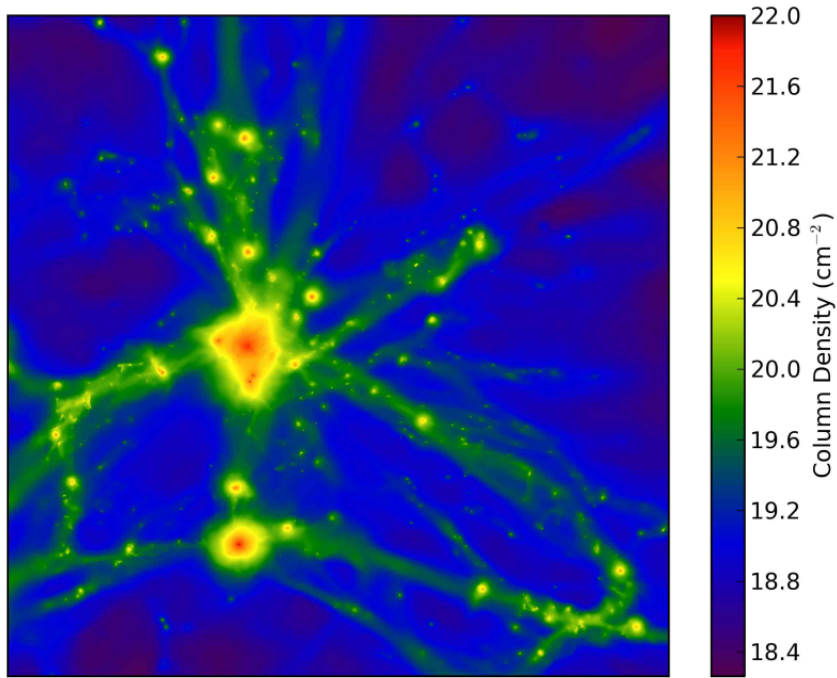


Figure 1.4: Gas density in Cen (2012) simulation showing similar distribution to filamentary network.

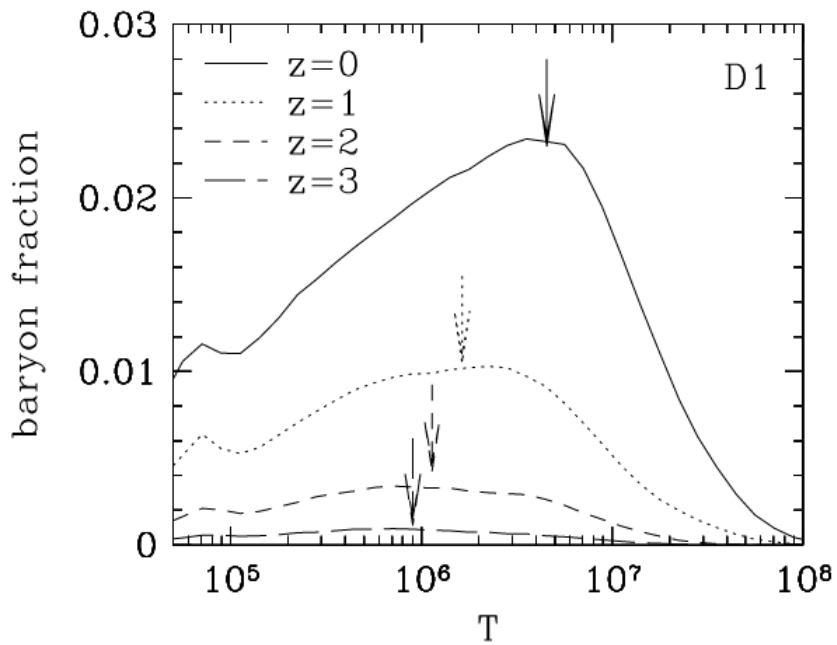


Figure 1.5: Mass fraction as a function on temperature shows that most local universe baryons are at temperature over $\log(T) = 6$ (Davé et al., 2001).

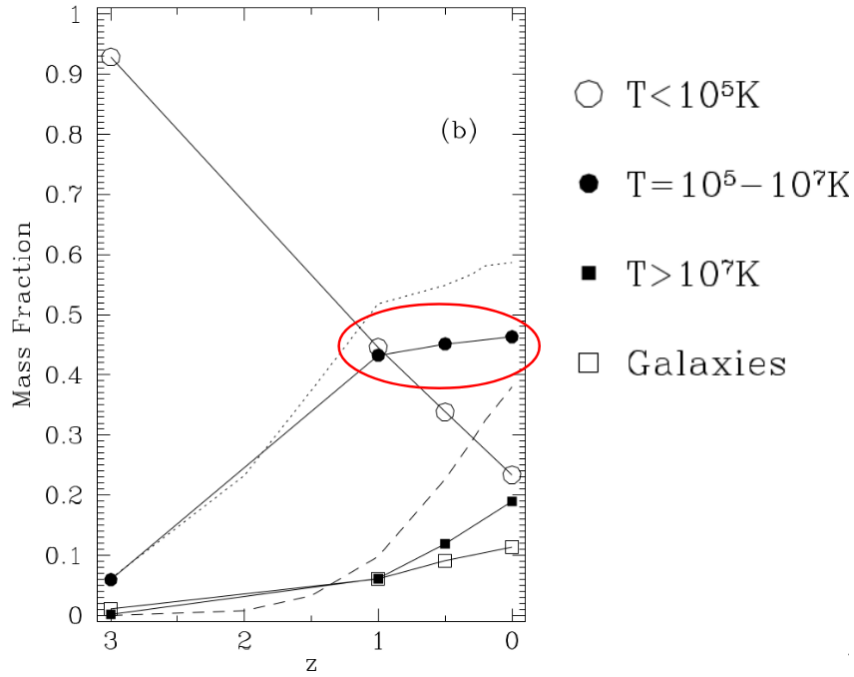


Figure 1.6: Mass fraction evolution showing almost half the baryons at WHIM temperatures (Cen, 2012).

1.3.2 WHIM correlation with luminosity

Following the assumption that galaxy distribution and WHIM is spatially correlated due to dominating dark matter gravitational potential, Nevalainen et al. (2015) studied the correlation between luminosity and WHIM density. First, the three-dimensional luminosity density field was calculated based on the spatial distribution and luminosities of the galaxies. The luminosities of galaxies are smoothed with symmetric kernel function to get the luminosity density and then the luminosity density is sampled in a grid to obtain the luminosity density field. The filamentary structure was constructed with Bisous model on simulation data. Restraining data close to the filament's spines increases WHIM mass fraction to $\rho_{\text{WHIM}} = 0.7\rho_{\text{b}}$, where ρ_{b} is baryon mass density. Nevalainen et al. (2015) show Pearson correlation coefficient of 0.8 between luminosity and WHIM density with 10^6 data points. From simulation data relation between WHIM density and luminosity density is derived as

$$\rho_{\text{WHIM}}(r) = 0.7 \times \left(\frac{\rho_{LD}(r)}{\langle \rho_{LD} \rangle} \right)^{0.9} \times \langle \rho_{\text{baryon}} \rangle, \quad (1.1)$$

where ρ_{WHIM} is WHIM density, ρ_{LD} luminosity density, $\langle \rho_{LD} \rangle$ mean luminosity density, and $\langle \rho_{\text{baryon}} \rangle$ mean baryonic density. The factor 0.7 takes into account that 70% baryons in filaments are WHIM.

Chapter 2

Observational methods

2.1 Filament detection

Sloan Digital Sky Survey (SDSS) is large spectroscopic survey including galaxy luminosities and redshifts (York et al., 2000). SDSS cover 17.5% (~ 7200 square degrees) of the whole sky. The sample consists of over a million galaxies and 100,000 quasars. In this work, we use smaller sample of the whole data. Only main contiguous area of the survey was used. Galaxies fainter than 17.77 were filtered out. Upper limit for constructing filaments is $z = 0.2$ and for further work $z = 0.07$ (and lower limit $z = 0.02$). The galaxy sample contains 584,449 objects. (Tempel et al., 2017)

Filamentary network is constructed on the SDSS data release 12 using the Bisous model (Tempel et al., 2017). This model was chosen, because it is specifically developed for observational data and does not need velocity field data, which is usually not obtained for spectroscopic surveys. Example of the configuration is seen on figure 2.1. Filament's radius is $r = 0.3 \dots 1.5 h^{-1} \text{Mpc}$, where $h = 70 \text{km s}^{-1} \text{Mpc}^{-1}$. Maximum length of a filament is $\sim 60 h^{-1} \text{Mpc}$. Most filaments have length below $10 h^{-1} \text{Mpc}$. (Tempel et al., 2014)

A spherical coordinates system named SDSS survey coordinates (η, λ) are used for representing the results in this work. Survey coordinates are covinient, when working with SDSS data as seen from figure 2.2. $(\eta, \lambda) = (0, 90)$ corresponds to $(\text{RA}, \text{dec}) = (275, 0)$, $(\eta, \lambda) = (57.5, 0)$ corresponds to $(\text{RA}, \text{dec}) = (0, 90)$, and $(\eta, \lambda) = (0, 0)$ corresponds to $(\text{RA}, \text{dec}) = (185, 32.5)$ (SDSS project, 1999).

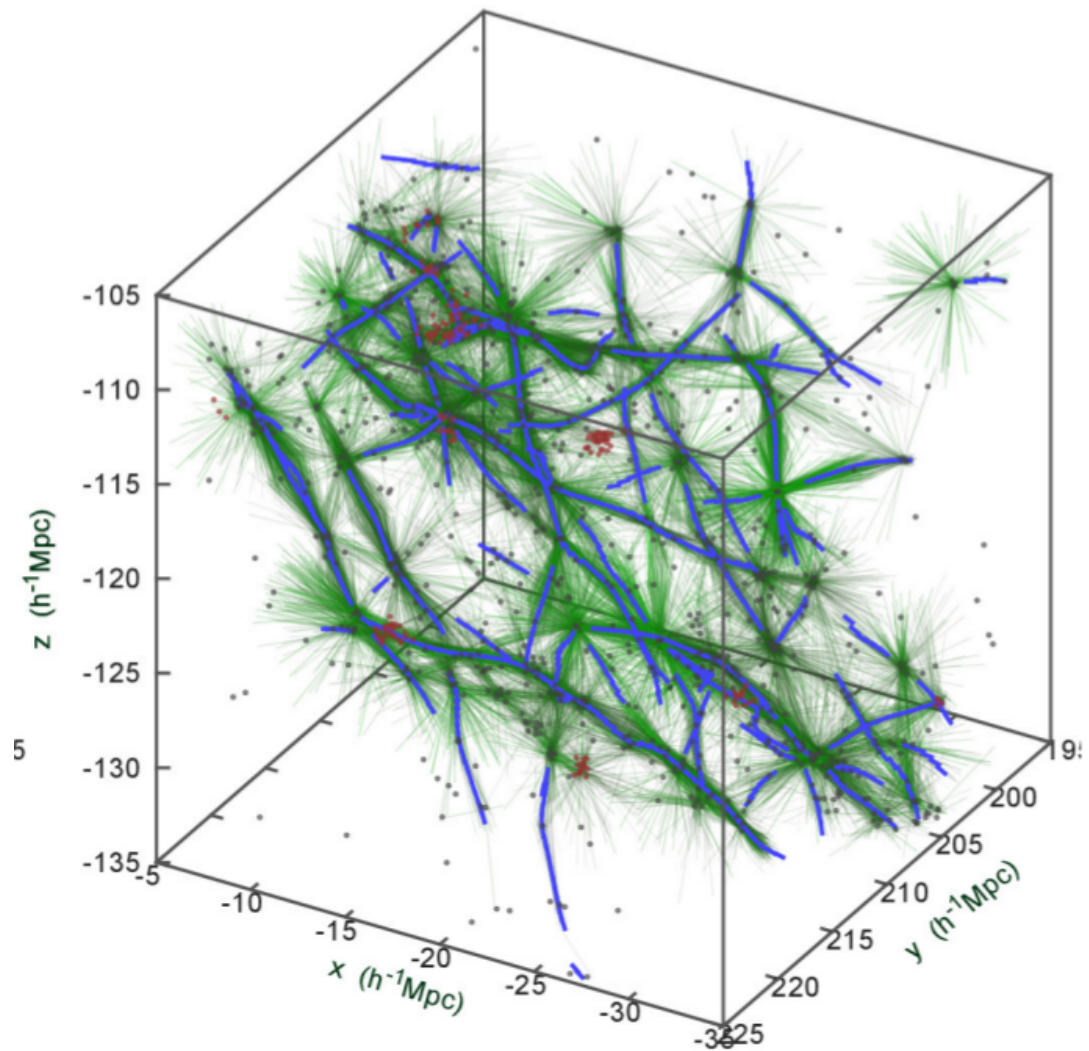


Figure 2.1: Example of filaments on SDSS data. Blue lines represent filament's spines, green lines visitmap, single galaxies marked with gray dots and groups with 10 galaxies and more red dots. (Tempel et al., 2014)

2.2 Identifying and characterizing the luminosity density structures

To use the correlation relation between luminosity and WHIM density on SDSS data, we have to find suitable luminosity structures. Following sections discuss how to define suitable luminosity structures and how to apply the correlation relation to find the WHIM density. For the X-ray follow-up, to observationally verify the results and detect WHIM structures, we are studying luminosity structures along the lines of sight, from which we get column densities. X-ray signal is proportional to the line of sight column density.

2.2.1 Lines of sight

In this work, we study luminosities along the lines of sight, which are defined in the area covered by SDSS (see figure 2.2). The lines of sight are chosen dispersedly over the area. In total 64 lines of sight were chosen with survey coordinates $\eta \in \{-20^\circ, -15^\circ, \dots, 15^\circ\}$, $\lambda \in \{-20^\circ, -15^\circ, \dots, 15^\circ\}$. The choice of lines of sight is random regarding the underlying physical properties. Each line of sight is presented in Cartesian coordinates with a step of 0.5 Mpc.

2.2.2 Crossing points

As the WHIM is located in the filamentary network, we must study structures that are close-by filament's spines. Filaments were detected in the SDSS data release 12 by Bisous model with parameters given in Tempel et al. (2016). Crossing points are defined as a line of sight points that are closer than 1 Mpc to a filament's spine. Crossing points are important to distinguish luminous structures in profiles that are generated by a separate bright galaxy or a group not belonging to the filamentary network. All the studied structures in this work have at least one crossing point, mostly more than one. Meaning all the studied structures are part of the filamentary network.

2.2.3 Structure identification from luminosity profiles

To construct the luminosity profile over the line of sight, we use the luminosities of galaxies in the SDSS spectroscopic data. The luminosity density profiles are calculated from galaxies' luminosities for a certain point in space. Profiles are calculated for distances 100 Mpc to 300

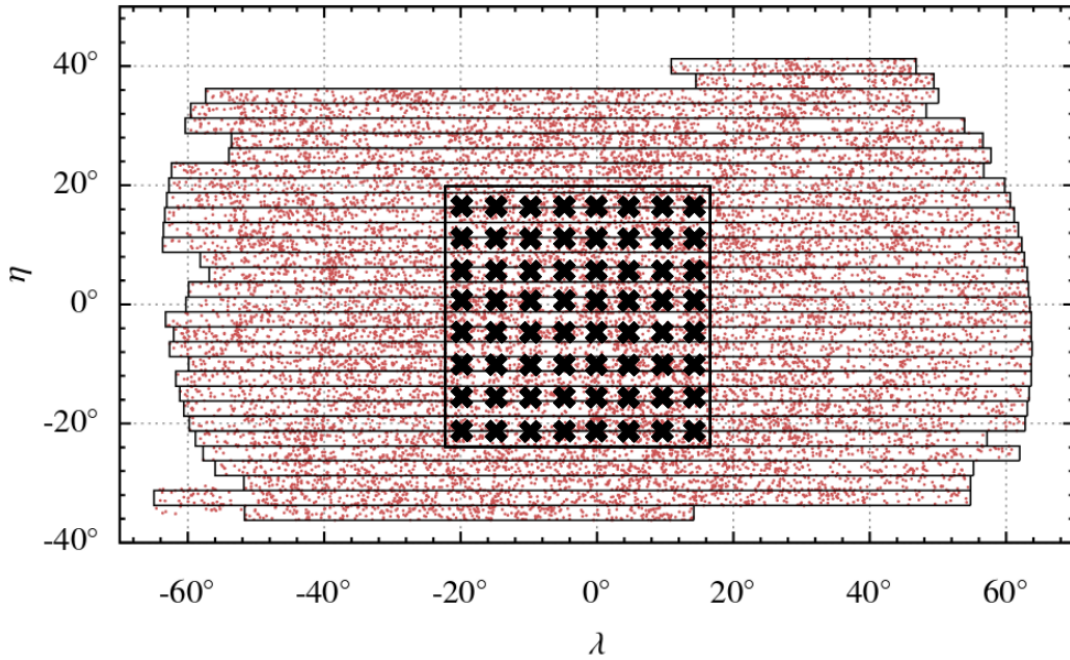


Figure 2.2: SDSS data release 7 sky coverage in survey coordinates λ , η . (Liivamägi et al., 2012) Data release 12 used in this work has the same coverage. Red dots are indicating galaxies. Black crosses indicate the coordinates of lines of sight. Rectangle is the area covered by this study.

Mpc with a constant step of 0.5 Mpc and smoothed with a kernel radius of 1.4 Mpc. Examples of profiles can be seen in figure 2.3. The distance is chosen according to the data. Although SDSS main galaxy sample extends further than 300 Mpc, the interval was chosen, where filaments detection is the most reliable.

A luminous structure is defined to have continuous luminosity higher than $0.01 \times 10^{10} L_{\odot} \text{Mpc}^{-3}$ but is allowed to have at most one radial bin with a lower value. This is to avoid dividing one structure into smaller ones that are next to each other. Defining structures is important, because not every luminous structure is connected to the filamentary network and using only structures with crossing points separates them. Connection to the filamentary network is important because the correlation between luminosity and WHIM density is applicable to WHIM in filaments.

2.2.4 WHIM column density

Having detected the luminous structures from the luminosity profiles of a line of sight, they can be characterized. Each structure is described by coordinates of the line of sight, mean distance from observer in CMB rest frame, length of the structure, the peak value of luminosity, WHIM

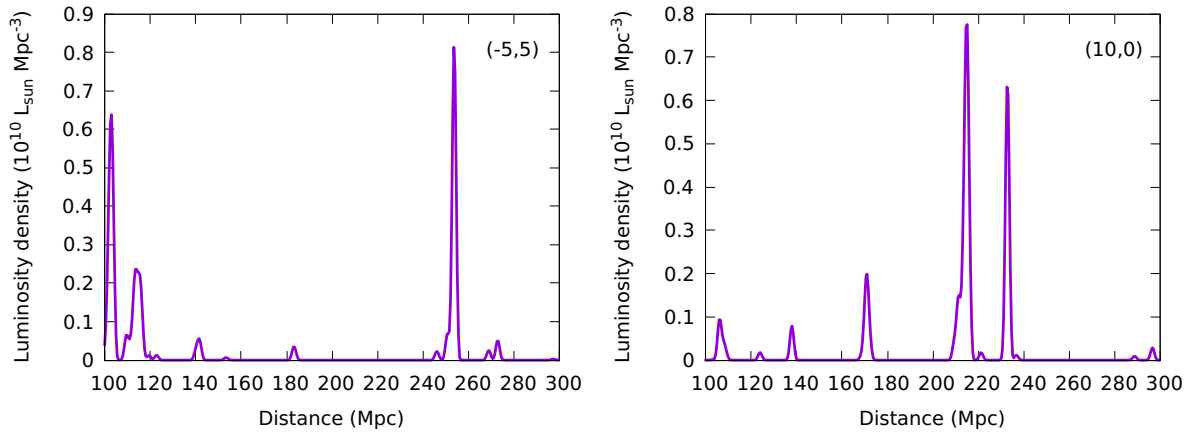


Figure 2.3: Luminosity density profiles over line of sight. Coordinates of line of sight left: $\eta = -5^\circ$ $\lambda = 5^\circ$, right: $\eta = 10^\circ$ $\lambda = 0^\circ$. Luminosity in physical units $L_\odot 10^{10} \text{Mpc}^{-3}$.

column density, and angle between filament's spine and line of sight.

Coordinates are in the form of SDSS survey coordinates (η, λ) . The peak value of luminosity is the highest value of luminosity along the line of sight within this structure.

WHIM column density is calculated based on the correlation between luminosity density and WHIM density in equation (1.1), where mean luminosity density $\langle \rho_{LD} \rangle$ for SDSS dataset is $0.01227 \times 10^{10} L_\odot \text{Mpc}^{-3}$ and mean baryonic density $\langle \rho_{\text{baryon}} \rangle$ for local universe is $0.617798 \times 10^{10} M_\odot \text{Mpc}^{-3}$ (Planck Collaboration et al., 2016). For WHIM column density we have to integrate over WHIM density line of sight (Nevalainen et al., 2015).

$$N_H(\text{WHIM}) = \int_{\text{struct}} \rho_{\text{WHIM}}(r) dr ,$$

where struct is the interval of distance, where structure is defined. WHIM column density gives an estimate of WHIM in a specific luminous structure and a way to compare different structures.

2.2.5 Oxygen abundance in WHIM structures

As ionized hydrogen has no absorption lines, we use oxygen ions to detect WHIM structures observationally, because oxygen is the third most common element in the universe. Although most heavier metals, including oxygen, reside in galaxies and clusters, supernovae and galactic wind carry it into the intergalactic medium. We can estimate the column densities for oxygen

ions in WHIM structures with equation

$$N(\text{ion}) = f_{\text{ion}}(T) \left(\frac{n(\text{el})}{n_H} \right)_{\text{solar}} A(\text{el}) \times N_H(\text{WHIM}), \quad (2.1)$$

where $f_{\text{ion}}(T)$ is the ionization fraction that depends on temperature, $\left(\frac{n(\text{el})}{n_H} \right)_{\text{solar}}$ is the ratio of number densities of given element and hydrogen in solar neighborhood measured from meteorites (Lodders et al., 2009), $A(\text{el})$ is abundance of given element in the filamentary environment. Ionization fraction f_{ion} is the given ion's number density ratio to total number density of the given element.

Based on the simulations roughly half of the WHIM mass is expected to be in the temperature range, where OVII absorption dominates (see figure 1.5 and 2.4). That means, in X-ray follow-up observations, about half of the structures identified in this work will be detected.

Using equation (2.1) we get the corresponding column density for OVII. The relative number density of oxygen is $\left(\frac{n(\text{O})}{n_H} \right)_{\text{solar}} \approx 10^{-3}$ (Lodders et al., 2009). There are no good observational results for the abundance of oxygen in intergalactic regions. It is known that oxygen abundance in the cluster outskirts is about 0.2 (Biffi et al., 2017). Clusters are situated at places, where filaments connect. At the cluster outskirts, we enter the filamentary environment. The smaller the density of supernovae in filaments the smaller the value of oxygen abundance. We use the commonly adopted value of $A(\text{O}) = 0.1$. The ionization fraction is $f_{\text{OVII}} \approx 1$ in a broad range around $\log(T) = 6$, where large fraction of WHIM is supposed to be. That gives OVII column density

$$N(\text{OVII}) \approx 10^{-4} \times N_H(\text{WHIM}). \quad (2.2)$$

The best detection limit for current X-ray instruments is $N(\text{OVII}) = 10^{16} \text{cm}^{-2}$, which means that we are not able to detect WHIM structures below $N_H(\text{WHIM}) = 10^{20} \text{cm}^{-2}$. With new X-ray observatories the limit will be lowered 10 times, meaning structures with $N_H(\text{WHIM}) = 10^{19} \text{cm}^{-2}$ could be detectable.

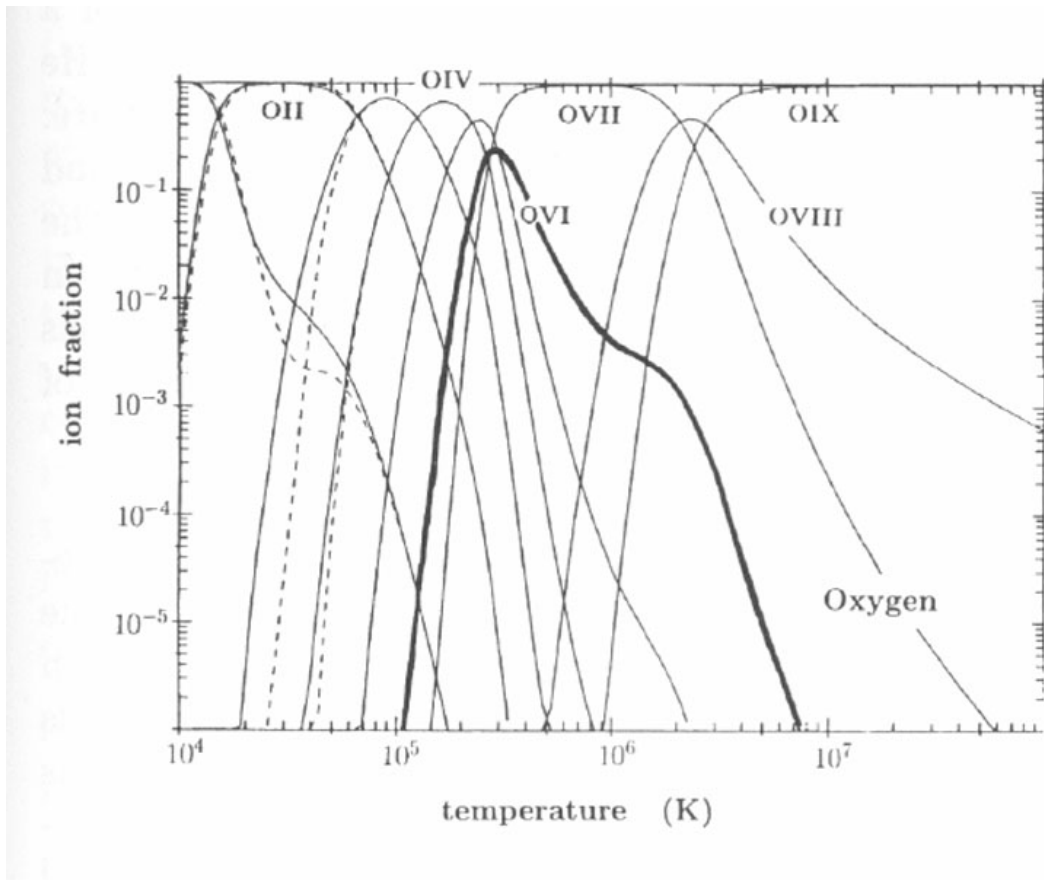


Figure 2.4: Oxygen ionization fractions as a function of temperature. Böhringer (1998)

Chapter 3

Results

3.1 Structures

3.1.1 Crossing points

Among 64 random lines of sight, there was one with no crossing points, the highest value was 33 nodes classified as crossing points on a line of sight (400 nodes), meaning that at most 8% of line of sight is closer than 1 Mpc to a filament's spine. In average there were 13.4 crossing point nodes on (3.35% of) a line of sight. See table 3.1 on how crossing points distribute among the lines of sight.

$n(cp)$	$\frac{n(cp)}{400} 100\%$	$n(los(> cp))$	$\frac{n(los(> cp))}{n(los)} 100\%$
5	1.25	51	79.7
10	2.5	35	54.7
15	3.75	24	37.5
20	5	13	20.3
25	6.25	8	12.5
30	7.5	5	7.8

Table 3.1: Crossing points (cp) distribution among lines of sight (los). $n(cp)$ is the number of crossing points on a line of sight, which corresponds to 0.5 Mpc of close-by filament. $\frac{n(cp)}{400} 100\%$ gives the percentage of line of sight radial bins (400) that has close-by filament spine for given number of crossing points. $n(los(> cp))$ is the number of lines of sight that have more than $n(cp)$ crossing points. $\frac{n(los(> cp))}{n(los)} 100\%$ is the percentage of lines of sight that have more than $n(cp)$ crossing points. This describes how much of lines of sight have close-by filaments, sorted by the distance of close-by filaments.

Property	Mean	Minimum	Maxium
Length (Mpc)	5.66	0.5	18.0
Luminosity peak value ($10^{10}L_{\odot}\text{Mpc}^{-3}$)	0.3257	0.0129	2.3990
Angle with spine ($^{\circ}$)	61.71	4.14	90.00
WHIM column density ($\text{cm}^{-2} \times 10^{19}$)	2.958	0.0531	18.648

Table 3.2: Properties of structure catalogue. Values of structure properties along the line of sight.

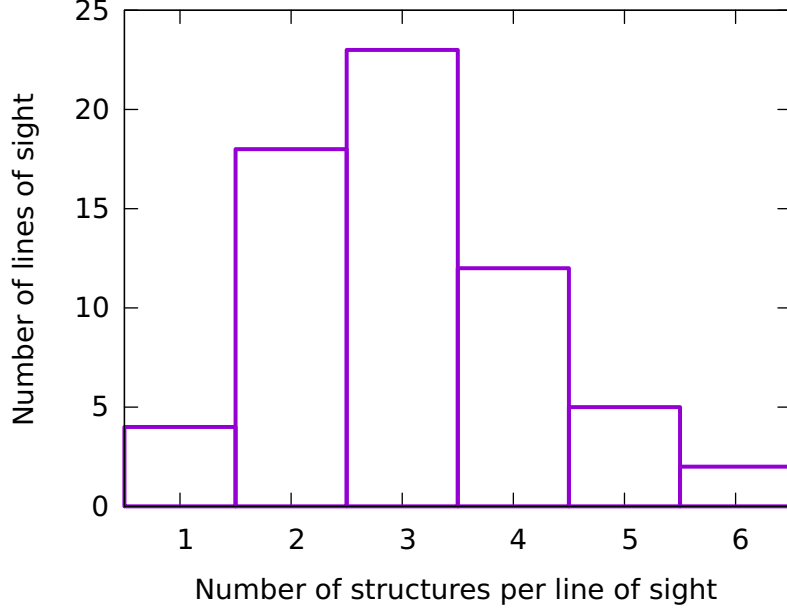


Figure 3.1: Distribution of 130 structures among the lines of sight.

3.1.2 Luminosity profiles

All the luminosity profiles of lines of sight were examined for structures and 130 were identified. See structure properties in table 3.2. All structure properties are measured along the line of sight, for example, structure length represent only structure's radial distance along the line of sight.

Luminosity profiles of four largest structures are given in figure 3.2. Their properties are seen in the table 3.3.

Coordinates	(5, 15)	(-5, 10)	(-15, 5)	(-20, 0)
Length (Mpc)	15.0	18.0	12.0	8.0
Mean distance (Mpc)	261	110	290	262
Luminosity peak value ($10^{10}L_{\odot}\text{Mpc}^{-3}$)	2.3990	0.4742	0.6515	2.3989
Angle with spine ($^{\circ}$)	49.4	25.8	28.6	39.4
WHIM column density ($\text{cm}^{-2} \times 10^{19}$)	18.648	10.851	12.559	16.531

Table 3.3: Structure properties of four brightest structures

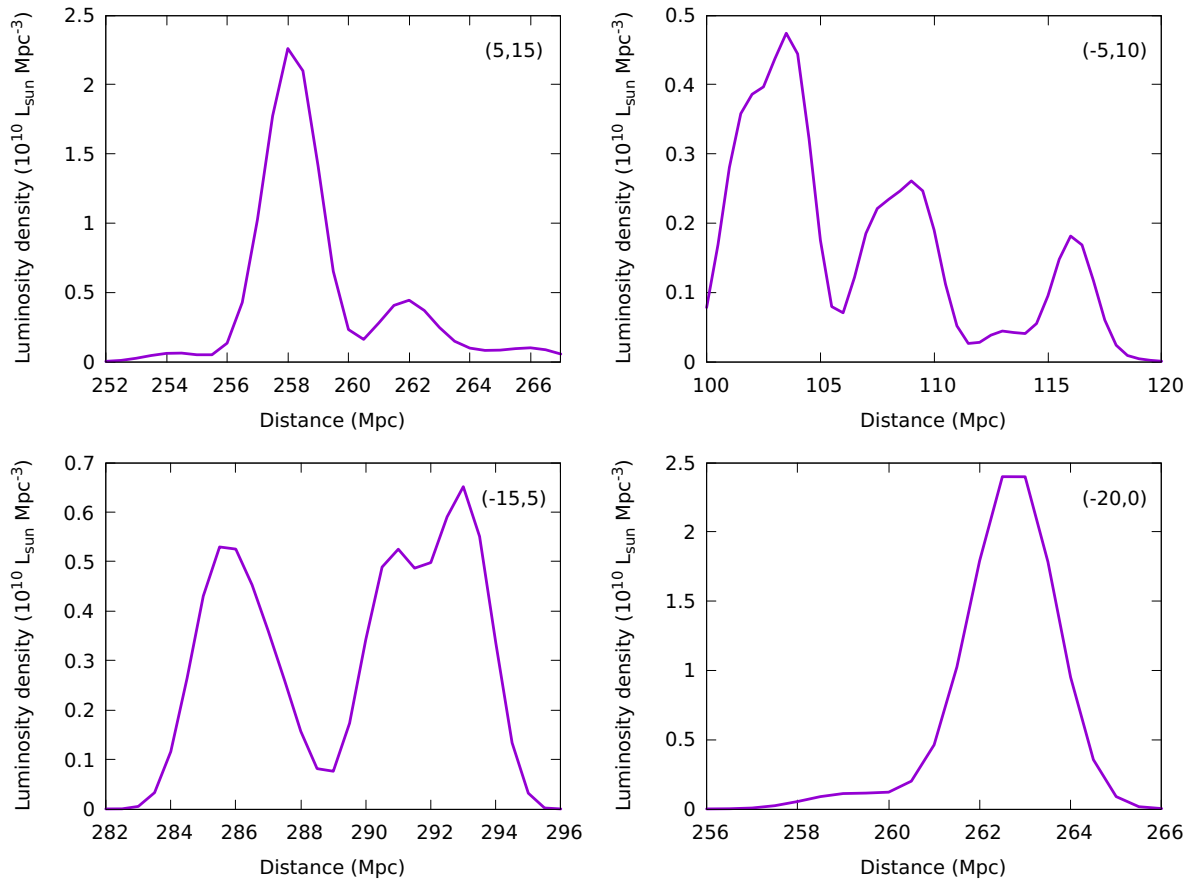


Figure 3.2: Luminosity profiles of four brightest structures. Upper row: $\eta = 5^\circ$, $\lambda = 15^\circ$ and $\eta = -5^\circ$, $\lambda = 10^\circ$. Lower row: $\eta = -15^\circ$, $\lambda = 5^\circ$ and $\eta = -20^\circ$, $\lambda = 0^\circ$.

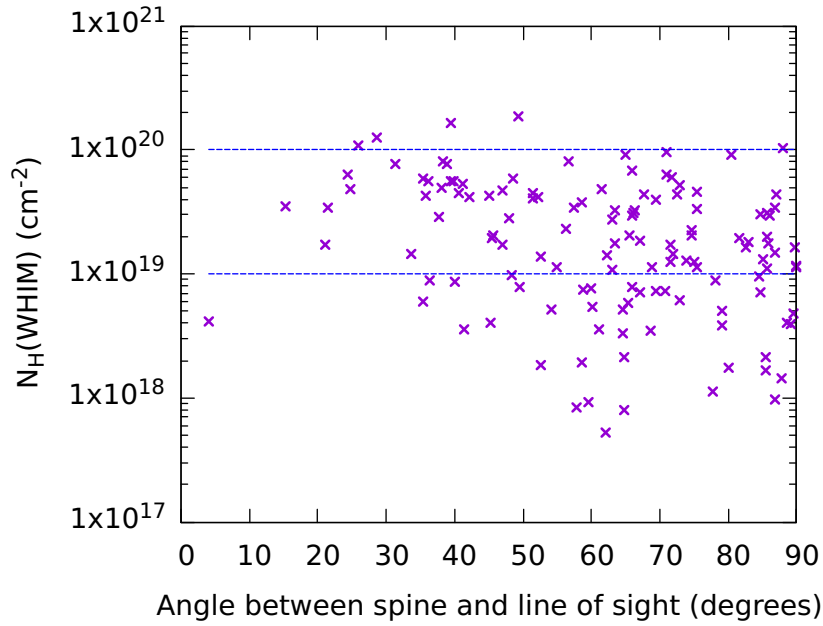


Figure 3.3: Column density distribution by angle between line of sight and filaments spine.

3.2 WHIM column density distribution and structure count

As WHIM follows filamentary network, the column density of a structure should depend on how well filament spine aligns with the line of sight. Assuming the structures are similar in other properties, the alignment with filament spine should positively affect the column density of the structure. We tested this by finding the angle between spine and line of sight at the point of crossing and plotting the distribution (see figure 3.3). As seen from the plot, there is no significant correlation between the angle and column density value. This shows that the angle is not strong enough factor to dominate the distribution. Other factors, such as structure size have a stronger influence.

Figure 3.4 shows the distribution of WHIM column densities. Higher values of WHIM column densities have less structures. There are 5 structures above $N_H(\text{WHIM}) > 10^{20} \text{ cm}^{-2}$ limit and 88 structures above $N_H(\text{WHIM}) > 10^{19} \text{ cm}^{-2}$ limit. We chose those limits, because these correspond to the detection limits of current and future instruments we plan to detect the structures with. Using equations (2.2) we can convert it to oxygen column densities (see table 3.4).

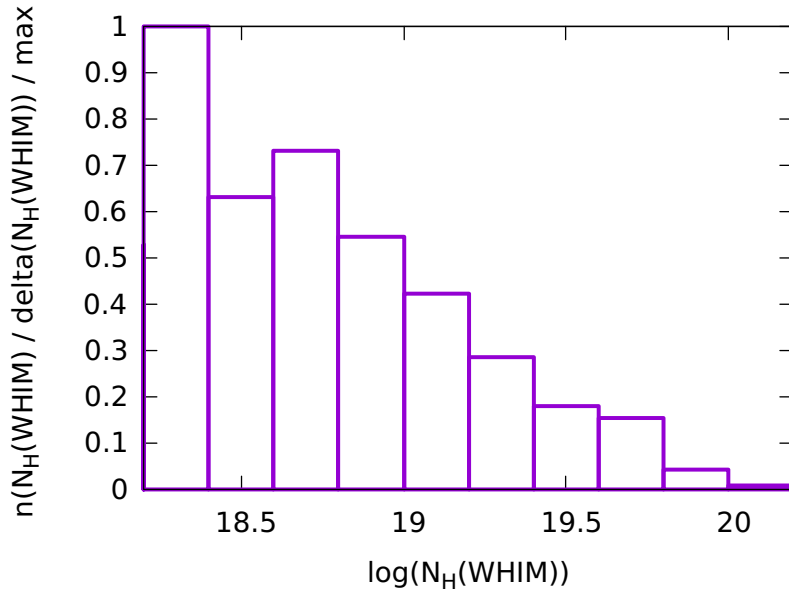


Figure 3.4: Y-axis shows the number of structures with WHIM column density in that interval divided by bin length and normalized. X-axis shows the WHIM column density bins of $\log(N_H(\text{WHIM})) = 0.2$. Column density distribution shows that structures with lower column density are more populous.

$N_H(\text{WHIM})$	$N(\text{OVII})$	Structures in studied area	Structures in whole SDSS	Structures in whole sky
10^{20}cm^{-2}	10^{16}cm^{-2}	5	23	129
10^{19}cm^{-2}	10^{15}cm^{-2}	88	396	2269

Table 3.4: Structure count with different column density limits for H and OVII. Column density for OVII ($N(\text{OVII})$) is important to compare the results with simulations as well as observationally for the X-ray follow-up.

3.3 Estimates for the whole sky

To generalize the results on the whole area surveyed by SDSS, we have to estimate the area covered by this study. Our goal is to find an area covered by each line of sight so that they don't overlap and count same structures multiple times. The lines of sight are 5° apart from one another. Taking that each line of sight covers a circular area around it with a radius of 2.5° (at the closest point of profiles, 100 Mpc, it converts to about 4.4 Mpc), which is the same magnitude as the structures (mean length of a structure is 5.66 Mpc). This means that we can consider the lines of sight cover the rectangular area as seen from figure 2.2. The area covered by the lines of sight is about 1600 square degrees. The whole SDSS area is 7221 square degrees, which gives us 22.2% coverage. Considering that on studied scales the structures in the SDSS

are uniformly distributed. We estimate the area covered by SDSS to have approximately 23 structures with $N_H(WHIM) > 10^{20}$ and 396 structures with $N_H(WHIM) > 10^{19}$. As the SDSS is a good representation of the whole sky, we can go even further. The number of structures for the whole sky can be calculated taking into account the area of the whole sky is 41253 square degrees (see table 3.4).

Chapter 4

Simulation results and follow-up observations

In order to test whether my estimates for the WHIM structure count are reasonable, we compare the predicted number of the WHIM structures with the estimates from the simulations of Cen (2012).

4.1 Comparison to simulations

Cen (2012) conducted a large-scale cosmological hydrodynamic simulation with a study of intergalactic OVII absorber distribution that can be used to compare verify the results of this work. As the luminosity density method doesn't specify the temperature of the WHIM we approximate that half of the found structures have temperatures, where OVII ionization fraction dominates. The main characteristic to compare with simulations is the number of structures found.

Using equations (2.2) OVII equivalent column densities can be found for WHIM. In this work, we found 88 structures above $N_H(\text{WHIM}) > 10^{19}\text{cm}^{-2}$. OVII equivalent column density is $N(\text{OVII}) = 10^{15}\text{cm}^{-2}$. Using figures 4.1 we can find structures for unit path length in redshift. As each line of sight studied in this work is 200 Mpc, the cumulative path length in this work is about $dz = 3.2$. For this path length, Cen (2012) simulation had roughly 30 OVII structures. This agrees with 44 OVII structures found in this work, considering half of all structures have dominant OVII absorption lines.

$$n(N_H(\text{WHIM}) > 10^{19}) \approx 50\% \times n(N(\text{OVII}) > 10^{15}) .$$

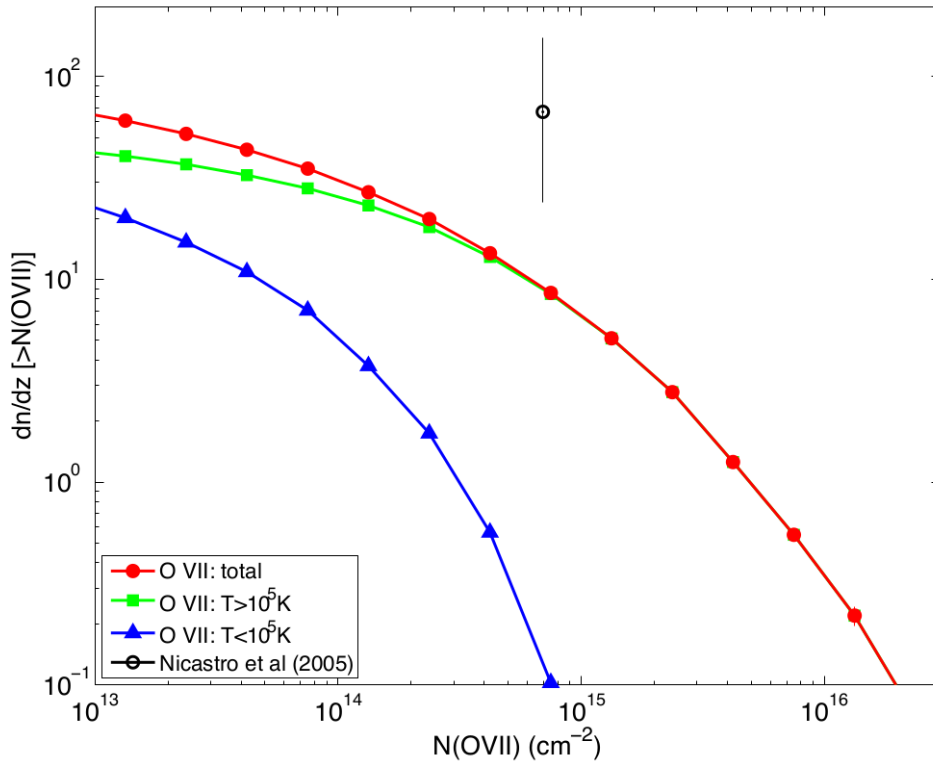


Figure 4.1: Cumulative OVII number density as a function of column density, defined as number of structures per unit redshift at the column density greater than the value at x-axis. Cen (2012)

4.2 X-ray observations

As discussed before, WHIM structures are traceable by OVII in the X-ray band. Two space telescopes with x-ray spectroscopy instruments, Chandra/LETG (Xue et al., 2011) and XMM-Newton/RGS (Brinkman et al., 1998; Jansen et al., 2001), are capable of detecting the signal from WHIM structures with OVII tracer. Both have good resolving efficiency at the OVII 20 Å line. The detection limit of current instruments is about $N(\text{OVII}) = 10^{16} \text{ cm}^{-2}$. That means there are about 65 WHIM structures (see table 3.4, half of the structures have OVII trace) in the whole sky detectable with these instruments. Future projects, ATHENA (Kaastra and Finoguenov, 2015) and ARCUS (Smith et al., 2016), increase the resolution by a magnitude. In addition, bigger effective area allows detecting the lines by a much smaller exposure time making it possible to cover a larger fraction of the sky with same exposure time as RGS. By increasing the resolution by magnitude, the number of detectable structures goes up to 1135.

Although we found a considerable amount of targets for X-ray absorption based on the column density values, observing those structures requires bright background blazars of which there are fewer than the structures. Gamma Ray Burst X-ray afterglows, if taking place behind the structures, can increase the number of observable X-ray absorption structures (Branchini et al.,

2009). That means the number of our observable structures is overestimated, but until further studies, this factor remains unknown.

Conclusions and further work

Cosmological simulations show that significant fraction of baryons is in the form of Warm-Hot Intergalactic Medium (Shull et al., 2012; Cen, 2012), that is hard to detect from spectroscopic survey due to diffuse gas and weak high energy absorption lines. The goal of this work was to study, when applying correlation between luminosity density and WHIM density (Nevalainen et al., 2015) to SDSS spectroscopic survey, if a reasonable amount of detectable WHIM structures are found. In this work, we applied the correlation on SDSS data release 12 using Bisous model (Tempel et al., 2014) to construct the filamentary network. This was successful, as the results produced numerous structures traceable by OVII absorption lines and agree with simulations. With current instruments 65 structures are detectable and with planned new instruments there are about 1000 detectable WHIM structures. As each structure is extended, X-ray observations of a structure may be feasible at several locations. This increases the odds of X-ray detection of WHIM structures.

Next step is to extend the study to the whole SDSS area, other spectroscopic surveys, and also to include OVI and OVIII tracers for finding WHIM structures. Because WHIM is intergalactic medium, clusters' and bright galaxies' influence on results should be studied in further detail to exclude any false positive WHIM structures found in this study. Next big goal is to put together a catalogue of detectable WHIM structures for spectroscopic surveys. For the catalogue, available bright background blazars have to be mapped and studied, as well as the Gamma Ray Bursts X-ray afterglow rates.

Acknowledgments

First, I am grateful for my supervisors Jukka Nevalainen and Elmo Tempel for guiding me, answering my questions and being persistent to keep me working. I learned a lot in addition to the subject of the thesis. I would like to thank Tartu Observatory and my colleagues there. Second, I appreciate the patience and help of my family and wife during the writing of this thesis.

Moorits Mihkel Muru

Bibliography

- Biffi, V., Planelles, S., Borgani, S., Fabjan, D., Rasia, E., Murante, G., Tornatore, L., Dolag, K., Granato, G. L., Gaspari, M., and Beck, A. M. (2017). The history of chemical enrichment in the intracluster medium from cosmological simulations. *MNRAS*, 468:531–548.
- Böhringer, H. (1998). Equilibrium Ionization and Non-Equilibrium Ionization Plasma Models. *IAU Colloq. 166: The Local Bubble and Beyond*, 506:341–352.
- Branchini, E., Ursino, E., Corsi, A., Martizzi, D., Amati, L., den Herder, J. W., Galeazzi, M., Gendre, B., Kaastra, J., Moscardini, L., Nicastro, F., Ohashi, T., Paerels, F., Piro, L., Roncarelli, M., Takei, Y., and Viel, M. (2009). Studying the Warm Hot Intergalactic Medium with Gamma-Ray Bursts. *ApJ*, 697:328–344.
- Brinkman, A., Aarts, H., den Boggende, A., Bootsma, T., Dubbeldam, L., den Herder, J., Kaastra, J., de Korte, P., van Leeuwen, B., Mewe, R., Paerels, F., de Vries, C., Cottam, J., Decker, T., Kahn, S., Rasmussen, A., Spodek, J., Branduardi-Raymont, G., Guttridge, P., Thomsen, K., Zehnder, A., and Guedel, M. (1998). The Reflection Grating Spectrometer onboard XMM. *Science with XMM*.
- Cen, R. (2012). Coincidences between O VI and O VII Lines: Insights from High-resolution Simulations of the Warm-hot Intergalactic Medium. *ApJ*, 753:17.
- Davé, R., Cen, R., Ostriker, J. P., Bryan, G. L., Hernquist, L., Katz, N., Weinberg, D. H., Norman, M. L., and O’Shea, B. (2001). Baryons in the Warm-Hot Intergalactic Medium. *ApJ*, 552:473–483.
- Jõeveer, M., Einasto, J., and Tago, E. (1978). Spatial distribution of galaxies and of clusters of galaxies in the southern galactic hemisphere. *MNRAS*, 185:357–370.
- Jansen, F., Lumb, D., Altieri, B., Clavel, J., Ehle, M., Erd, C., Gabriel, C., Guainazzi, M., Gondoin, P., Much, R., Munoz, R., Santos, M., Schartel, N., Texier, D., and Vacanti, G. (2001). XMM-Newton observatory. I. The spacecraft and operations. *Astronomy & Astrophysics*, 365:L1–L6.

- Kaastra, J. and Finoguenov, A. (2015). The missing baryons and the warm-hot intergalactic medium. *Exploring the Hot and Energetic Universe: The first scientific conference dedicated to the Athena X-ray observatory*, page 12.
- Komatsu, E., Smith, K. M., Dunkley, J., Bennett, C. L., Gold, B., Hinshaw, G., Jarosik, N., Larson, D., Nolte, M. R., Page, L., Spergel, D. N., Halpern, M., Hill, R. S., Kogut, A., Limon, M., Meyer, S. S., Odegard, N., Tucker, G. S., Weiland, J. L., Wollack, E., and Wright, E. L. (2011). Seven-year Wilkinson Microwave Anisotropy Probe (WMAP) Observations: Cosmological Interpretation. *ApJS*, 192:18.
- Libeskind, N. I., Hoffman, Y., Knebe, A., Steinmetz, M., Gottlöber, S., Metuki, O., and Yepes, G. (2012). The cosmic web and the orientation of angular momenta. *MNRAS*, 421:L137–L141.
- Libeskind, N. I., van de Weygaert, R., Cautun, M., Falck, B., Tempel, E., Abel, T., Alpaslan, M., Aragón-Calvo, M. A., Forero-Romero, J. E., Gonzalez, R., Gottlöber, S., Hahn, O., Hellwing, W. A., Hoffman, Y., Jones, B. J. T., Kitaura, F., Knebe, A., Manti, S., Neyrinck, M., Nuza, S. E., Padilla, N., Platen, E., Ramachandra, N., Robotham, A., Saar, E., Shandarin, S., Steinmetz, M., Stoica, R. S., Sousbie, T., and Yepes, G. (2018). Tracing the cosmic web. *MNRAS*, 473:1195–1217.
- Liivamägi, L. J., Tempel, E., and Saar, E. (2012). SDSS DR7 superclusters. The catalogues. *Astronomy & Astrophysics*, 539:A80.
- Lodders, K., Palme, H., and Gail, H.-P. (2009). 4.4 abundances of the elements in the solar system: Datasheet from landolt-börnstein - group vi astronomy and astrophysics · volume 4b: “solar system”.
- Nevalainen, J., Tempel, E., Liivamägi, L. J., Branchini, E., Roncarelli, M., Giocoli, C., Heinämäki, P., Saar, E., Tamm, A., Finoguenov, A., Nurmi, P., and Bonamente, M. (2015). Missing baryons traced by the galaxy luminosity density in the large-scale whim filaments. *Astronomy & Astrophysics*, 583:A142.
- Planck Collaboration, Ade, P. A. R., Aghanim, N., Arnaud, M., Ashdown, M., Aumont, J., Baccigalupi, C., Banday, A. J., Barreiro, R. B., Bartlett, J. G., and et al. (2016). Planck 2015 results. XIII. Cosmological parameters. *Astronomy & Astrophysics*, 594:A13.
- SDSS project (1999). SDSS Survey coordinates. <http://www.sdss.org/dr12/algorithms/surveycoords/>. Last checked on 03.06.2018.
- Shull, J. M., Smith, B. D., and Danforth, C. W. (2012). The Baryon Census in a Multiphase Intergalactic Medium: 30% of the Baryons May Still be Missing. *ApJ*, 759:23.

- Smith, R. K., Abraham, M. H., Allured, R., Bautz, M., Bookbinder, J., Bregman, J. N., Brennenman, L., Brickhouse, N. S., Burrows, D. N., Burwitz, V., Carvalho, R., Cheimets, P. N., Costantini, E., Dawson, S., DeRoo, C., Falcone, A., Foster, A. R., Grant, C. E., Heilmann, R. K., Hertz, E., Hine, B., Huenemoerder, D., Kaastra, J. S., Madsen, K. K., McEntaffer, R. L., Miller, E. D., Miller, J., Morse, E., Mushotzky, R., Nandra, K., Nowak, M., Paerels, F., Petre, R., Plice, L., Poppenhaeger, K., Ptak, A., Reid, P., Sanders, J., Schattenburg, M. L., Schulz, N., Smale, A., Temi, P., Valencic, L., Walker, S., Willingale, R., Wilms, J., and Wolk, S. J. (2016). Arcus: the x-ray grating spectrometer explorer. *Space Telescopes and Instrumentation 2016: Ultraviolet to Gamma Ray*, 9905:99054M.
- Tempel, E., Stoica, R. S., Kipper, R., and Saar, E. (2016). Bisous model-Detecting filamentary patterns in point processes. *Astronomy and Computing*, 16:17–25.
- Tempel, E., Stoica, R. S., Martínez, V. J., Liivamägi, L. J., Castellan, G., and Saar, E. (2014). Detecting filamentary pattern in the cosmic web: a catalogue of filaments for the SDSS. *MNRAS*, 438:3465–3482.
- Tempel, E., Tuvikene, T., Kipper, R., and Libeskind, N. I. (2017). Merging groups and clusters of galaxies from the SDSS data. The catalogue of groups and potentially merging systems. *Astronomy & Astrophysics*, 602:A100.
- Xue, Y. Q., Luo, B., Brandt, W. N., Bauer, F. E., Lehmer, B. D., Broos, P. S., Schneider, D. P., Alexander, D. M., Brusa, M., Comastri, A., Fabian, A. C., Gilli, R., Hasinger, G., Hornschemeier, A. E., Koekemoer, A., Liu, T., Mainieri, V., Paolillo, M., Rafferty, D. A., Rosati, P., Shemmer, O., Silverman, J. D., Smail, I., Tozzi, P., and Vignali, C. (2011). The Chandra Deep Field-South Survey: 4 Ms Source Catalogs. *ApJS*, 195:10.
- York, D. G. et al. (2000). The Sloan Digital Sky Survey: Technical Summary. *AJ*, 120:1579–1587.

Lihtlitsents lõputöö reprodutseerimiseks ja lõputöö üldsusele kättesaadavaks tegemiseks

Mina, Moorits Mihkel Muru,

1. annan Tartu Ülikoolile tasuta loa (lihtlitsentsi) enda loodud teose

Detection of WHIM structure candidates in the SDSS spectroscopic survey,

mille juhendajad on Jukka Henry Petteri Nevalainen, PhD ja Elmo Tempel, PhD,

- (a) reprodutseerimiseks säilitamise ja üldsusele kättesaadavaks tegemise eesmärgil, sealhulgas digitaalarhiivi DSpace-is lisamise eesmärgil kuni autoriõiguse kehtivuse tähtaja lõppemiseni;
 - (b) üldsusele kättesaadavaks tegemiseks Tartu Ülikooli veebikeskkonna kaudu, sealhulgas digitaalarhiivi DSpace'i kaudu kuni autoriõiguse kehtivuse tähtaja lõppemiseni.
2. olen teadlik, et punktis 1 nimetatud õigused jäävad alles ka autorile.
 3. kinnitan, et lihtlitsentsi andmisega ei rikuta teiste isikute intellektuaalomandi ega isikuandmete kaitse seadusest tulenevaid õigusi.